Physics in Collision - Zeuthen, Germany, June 26-28, 2003

NEUTRINO OSCILLATIONS: A GLOBAL ANALYSIS

G.L. Fogli, E. Lisi, A. Marrone, D. Montanino*, A. Palazzo, A.M. Rotunno
Dipartimento di Fisica & Sezione INFN, Bari
**Dipartimento di Fisica & Sezione INFN, Lecce*

ABSTRACT

We review the status of the neutrino oscillation physics (as of June 2003), with a particular emphasis on the present knowledge of the neutrino mass-mixing parameters in a three generation approach. We consider first the $\nu_\mu \to \nu_\tau$ flavor transitions of atmospheric neutrinos. It is found that standard oscillations provide the best description of the SK+K2K data, and that the associated mass-mixing parameters are determined at $\pm 1\sigma$ (and $N_{\rm DF} = 1$) as: $\Delta m^2 = (2.6 \pm 0.4) \times 10^{-3}$ eV^2 and $\sin^2 2\theta = 1.00^{+0.00}_{-0.05}$. Such indications, presently dominated by SK, could be strengthened by further K2K data. Then we analyze the energy spectrum of reactor ν events recently observed at KamLAND and combine them with solar and terrestrial ν data. We find that the solution to the solar ν problem at large mixing angle (LMA) is basically split into two sub-regions, that we denote as LMA-I and LMA-II. The LMA-I solution, characterized by lower values of the squared neutrino mass gap, is favored by the global data fit. Finally, we briefly illustrate how prospective data from the SNO and KamLAND can increase our confidence in the occurrence of standard matter effects in the Sun, which are starting to emerge from current data.

1 Introduction

In its first phase of operation (years 1996–2001), the Super-Kamiokande (SK) experiment has provided, among other important results, compelling evidence for atmospheric ν_μ disappearance [1, 2]. This evidence, now firmly based on a high-statistics 92 kton-year exposure [3], has not only been corroborated by consistent indications in the MACRO [4] and Soudan 2 [5] atmospheric neutrino experiments, but has also been independently checked by the first long-baseline KEK-to-Kamioka (K2K) accelerator experiment [6, 7], using SK as a target for ν_μ's produced 250 km away with $\langle E_\nu \rangle \sim 1.3$ GeV. Neutrino flavor oscillations, interpreted in terms of nonzero mass-mixing parameters $(\Delta m^2, \sin^2 2\theta)$ in the $\nu_\mu \to \nu_\tau$ channel, provide by far the best and most natural explanation for the observed ν_μ disappearance [1, 2].

In Section 2 we review the phenomenological status of the standard oscillations in the $\nu_\mu \to \nu_\tau$ channel, in the light of the latest SK atmospheric zenith distributions [3] and of the first spectral results from the K2K experiment [7].

On the solar neutrino front, the Chlorine [8], Gallium [9, 10, 11], Super-Kamiokande (SK) [12, 13] and Sudbury Neutrino Observatory (SNO) [14, 15, 16] solar neutrino experiments have convincingly established that the deficit of the observed solar ν_e flux with respect to expectations [17] implies new neutrino physics. In particular, the charged and neutral current (CC and NC) data from SNO have proven the occurrence of ν_e transitions into a different active state ν_a with a statistical significance greater than 5σ [15].

Barring sterile neutrinos and nonstandard ν interactions, such transitions can be naturally explained by the hypothesis of flavor oscillations [18] in the $\nu_e \to \nu_a$ channel (ν_a being a linear combination of ν_μ and ν_τ) driven by nonzero ν squared mass difference and mixing angle parameters $(\delta m^2, \theta_{12})$ [19]. The (ν_μ, ν_τ) combination orthogonal to ν_a is probed by atmospheric ν oscillations [2], with different parameters $(\Delta m^2, \theta_{23})$ [20]. The third mixing angle θ_{13}, needed to complete the 3×3 mixing matrix, is constrained to be small by additional reactor results [21, 22], and can be set to zero to a good approximation for our purposes.

The recent results from the Kamioka Liquid scintillator AntiNeutrino Detector (KamLAND) [23] have provided a beautiful and crucial confirmation of the solar ν_e oscillation picture through a search for long-baseline oscillations of reactor $\overline{\nu}_e$'s. The observed of $\overline{\nu}_e$ disappearance in KamLAND has confirmed the previously favored solution in the $(\delta m^2, \theta_{12})$ parameter space, often referred to as the large mixing angle (LMA) region [16] in the literature (see, e.g., [24] and references therein). Moreover, the KamLAND data have basically split this region into two

allowed subregions, which we will refer to as LMA-I and LMA-II, following Ref. [25].

In Sections 3 we analyze the first KamLAND spectral data [23] and combine them with current solar neutrino data [8, 9, 10, 11, 13, 14, 15, 16], assuming two-flavor oscillations of active neutrinos [24], in order to determine the surviving sub-regions of the LMA solution. In the analysis we include the CHOOZ reactor data [21].

Finally, in Section 4 we briefly illustrate how emerging indications of solar matter effects can be corroborated in the LMA parameter region. In particular, we show that the amplitude of matter effects (introduced as a free parameter $a_{\rm MSW}$) can be significantly constrained by using prospective data from SNO and KamLAND.

2 "Atmospheric" neutrinos

A careful analysis of the SK and K2K data sets used in the following can be found in [26]. Concerning SK atmospheric neutrino data (92 kton-year [3]), we use the usual zenith angle (θ_z) distributions of leptons: sub-GeV e-like and μ-like events, divided in 10+10 bins; multi-GeV e-like and μ-like events, divided in 10+10 bins; upward stopping and through-going μ events, divided in 5+10 bins. The calculation of the theoretical events rates $R_n^{\rm theo}$ in each of the 55 bins is done as in [27, 28, 29]. The SK statistical analysis is considerably improved with respect to [27, 29]. Now the set of systematic errors has been enlarged to 11 entries, leading to a more complex structure of correlated errors affecting the $R_n^{\rm theo}$'s, as emphasized in [30].

Concerning the K2K data, we use the absolute spectrum of muon events in terms of the reconstructed neutrino energy E [7], which provides a total of 29 events (here divided in 6 bins). In this sample, the parent neutrino interactions are dominantly quasi-elastic (QE), and the reconstructed energy E is thus closely correlated with the true neutrino energy E_ν.

Let us now discuss the updated bounds on the parameters (Δm^2, $\sin^2 2\theta$), governing the scenario of standard oscillations (here $\theta = \theta_{23}$).

Fig. 1 shows the joint bounds on the (Δm^2, $\sin^2 2\theta$) parameters from our analysis of SK, K2K, and SK+K2K data. The bounds in the left panel are very close to the official SK ones, as presented in [3]. The bounds in the middle panel are instead slightly weaker than the official K2K ones [7], especially in terms of $\sin^2 2\theta$. In particular, we do not find a lower bound on $\sin^2 2\theta$ at 99% C.L. (for $N_{\rm DF} = 2$). The reason is that we cannot use the additional (dominantly) non-QE event sample of K2K (27 events), which would help to constrain the overall rate normalization and thus $\sin^2 2\theta$. This fact might also explain why we find the K2K best fit at

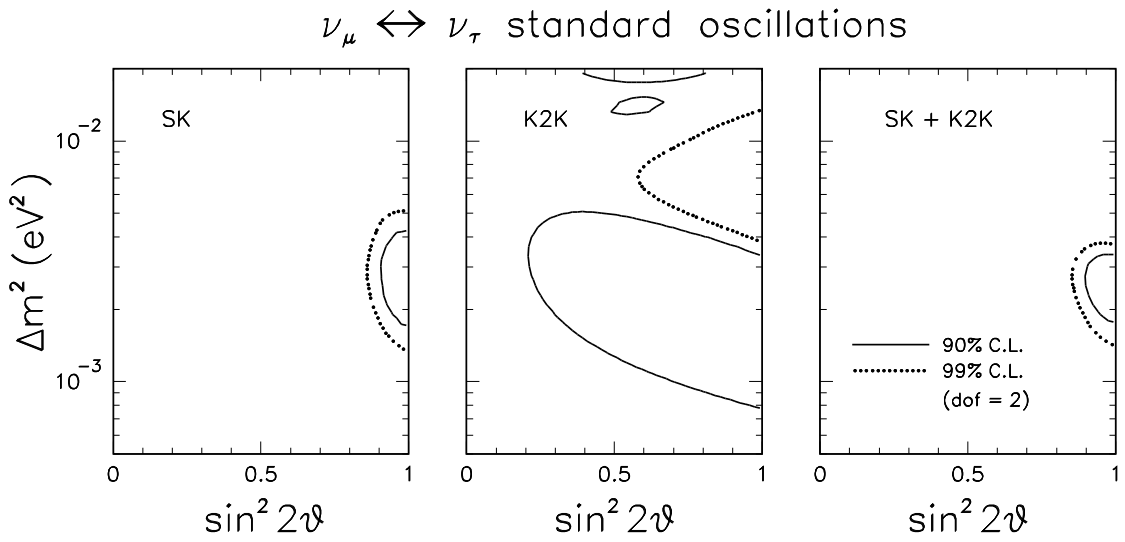

Figure 1: *Standard oscillations in the $\nu_\mu \to \nu_\tau$ channel: bounds on the parameters $(\Delta m^2, \sin^2 2\theta)$ from SK atmospheric data (left panel), K2K spectral data (middle panel), and their combination (right panel).*

$\sin^2 2\theta = 0.82$ rather than at 1.00 as in [7]. By comparing the left and right panels of Fig. 1, the main effect of K2K appears to be the strengthening of the upper bound on Δm^2, consistently with the trend of the first K2K data (rate only [6], no spectrum) [29]. The main reason is that, for $\Delta m^2 \sim (4\text{–}6) \times 10^{-3}$ eV^2, the first oscillation minimum would be located at—or just above—the K2K energy spectrum peak, implying a strong local and overall suppression of the expected events.

Fig. 2 shows on the left the SK and SK+K2K bounds on Δm^2, when the $\sin^2 2\theta$ parameter is projected (minimized) away. The linear scale in Δm^2 makes the K2K impact on the upper limit more evident. Notice that, up to $\sim 3\sigma$, the global (SK+K2K) χ^2 function is approximately parabolic in the *linear* variable Δm^2, so that one can define a one- standard-deviation error for this parameter. This feature was already argued on the basis of a graphical reduction of the official SK and K2K likelihood functions [24], and is here confirmed through a full analysis. By keeping only the first significant figure in the error estimate, a parabolic fit provides the $\pm 1\sigma$ range

$$\Delta m^2 = (2.6 \pm 0.4) \times 10^{-3} \text{ eV}^2 \ . \tag{1}$$

The bounds on $\sin^2 2\theta$ are instead entirely dominated by SK. This is shown on the right of Fig. 3, where the $\Delta\chi^2$ function in terms of $\sin^2 2\theta$ is reported, for Δm^2 projected (minimized) away in the SK fit. Here the addition of K2K data would insignificantly change the bounds (not shown), which thus hold for both the

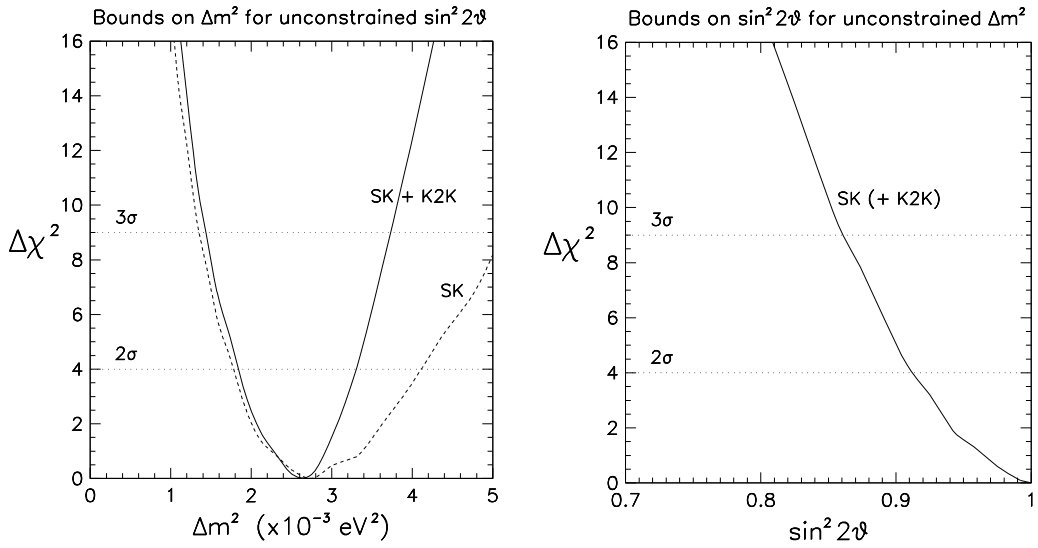

Figure 2: *Standard oscillations in the $\nu_\mu \to \nu_\tau$ channel. On the left: bounds on Δm^2 for unconstrained* $\sin^2 2\theta$ *from SK (dashed curve) and SK+K2K (solid curve). On the right: bounds on* $\sin^2 2\theta$ *for unconstrained Δm^2 from SK data. The inclusion of K2K data induces here negligible changes (not shown).*

SK and the SK+K2K fit. Also in this case, the nearly parabolic behavior of $\Delta\chi^2$ allows to properly define a 1σ range,

$$\sin^2 2\theta = 1.00^{+0.00}_{-0.05} \ , \tag{2}$$

with the lower $N\sigma$ error scaling linearly with N (up to $N \simeq 3$). Equations (1) and (2) concisely review the current fit to the standard oscillation parameters, as anticipated in the Introduction.

Fig. 3 shows the comparison between observations and best-fit predictions for the SK zenith distributions. In particular, the comparison between solid and dashed histograms shows that the systematic shifts are often comparable in size to the statistical errors, implying that just increasing the SK atmospheric ν statistics will hardly bring decisive new information on the standard oscillation scenario. In the SG and MG samples, the fit clearly exploits the systematic uncertainties to increase the e-like event normalization, especially in the upward direction, so as to reduce the "electron excess" possibly indicated by SK data.

Concerning μ-like events in the SG and MG samples, the fit shows an opposite tendency to slightly decrease the normalization of (especially down-going) events. The tendency appears to be reversed in the high-energy UT sample. Taken together, these opposite shifts of e-like and μ-like expectations in the SG and MG

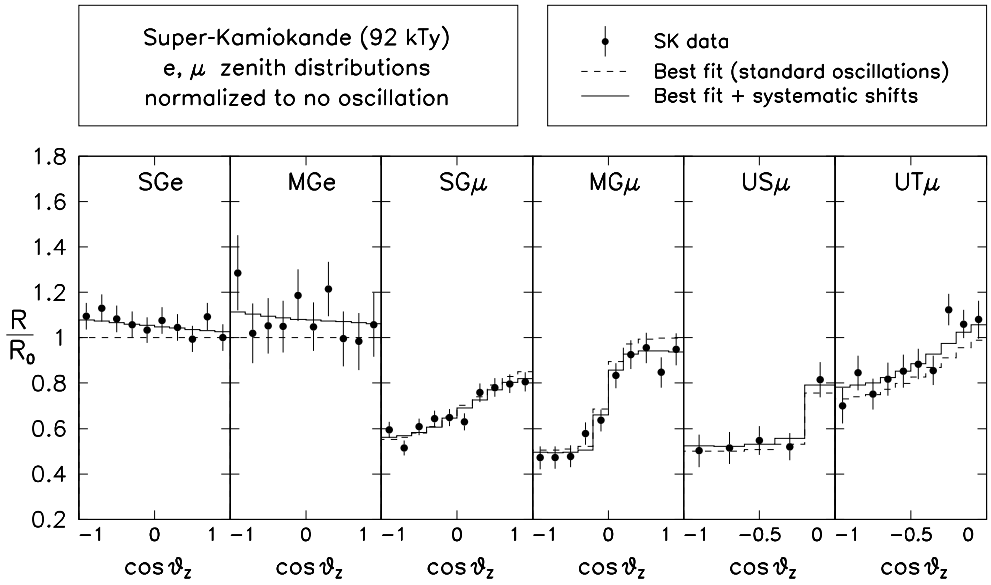

Figure 3: *SK experimental zenith distributions ($\pm 1\sigma_{\rm stat}$), compared with the corresponding theoretical ones at the global (SK+K2K) best-fit point. All distributions are normalized to the unoscillated predictions in each bin. For the theoretical event rates, we show both the central values $R_n^{\rm theo}$ (dashed histograms) and the "shifted" values $\overline{R}_n^{\rm theo}$ (solid histograms), which embed the effect of systematic pulls. The difference between $\overline{R}_n^{\rm theo}$ and $R_n^{\rm theo}$ shows how much (and in which direction) the correlated systematic errors tend to stretch the predictions in order to match the data.*

samples seem to suggest some systematic deviation from the predicted μ/e flavor ratio which, although not statistically alarming, should be kept in mind: deviations of similar size might have their origin in neutrino physics beyond 2ν oscillations. Unfortunately, since such effects are typically not larger than the systematic shifts in Fig. 3, they are likely to remain hidden in higher-statistics SK data.

3 Impact of KamLAND on solar neutrinos (a 2ν analysis)

The KamLAND recent observation of $\overline{\nu}_e$ disappearance [23] confirms the current interpretation of solar neutrino data [13, 16, 24, 30] in terms of $\nu_e \to \nu_{\mu,\tau}$ oscillations induced by neutrino mass and mixing [18, 19], and restricts the corresponding parameter space $(\delta m^2, \theta_{12})$ within the so-called large mixing angle (LMA) region. In this region, globally favored by solar neutrino data, matter effects [31, 32] in adiabatic regime [33, 31] are expected to dominate the dynamics of flavor transitions in the Sun (see, e.g., [34]). The KamLAND spectral data appear to exclude some significant portions of the LMA solution [23], where the predicted spectrum

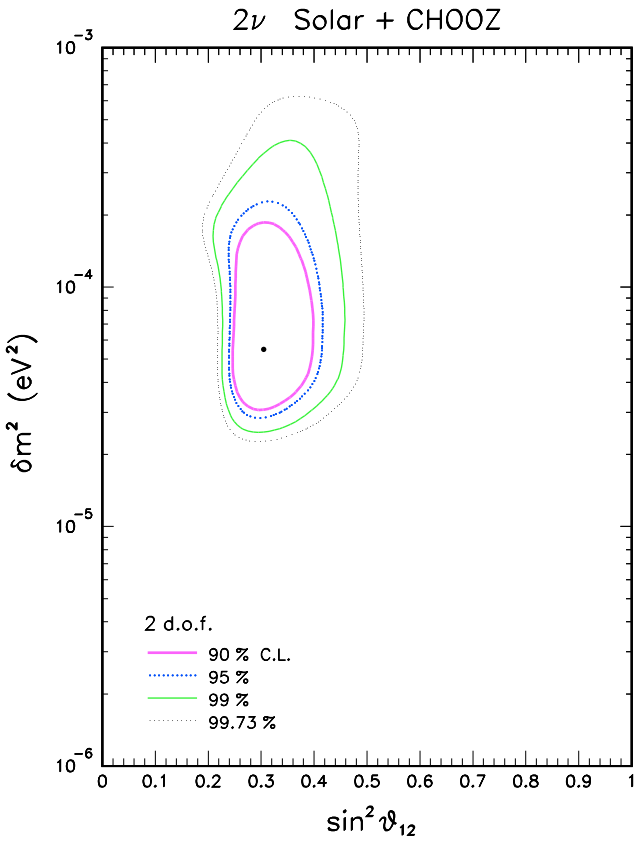

Figure 4: *Two-flavor active neutrino oscillations: Global analysis of solar and CHOOZ neutrino data in the* $(\delta m^2, \sin^2\theta_{12})$ *parameter space, restricted to the LMA region. The best fit is indicated by a black dot.*

distortions [24] would be in conflict with observations [23].

In the 2ν case, we find that the inclusion of the KamLAND spectrum basically splits the LMA solution into two sub-regions at "small" and "large" δm^2, which we call LMA-I and LMA-II, respectively (the LMA-I solution being preferred by the data) [35]. Such regions are only slightly modified in the presence of 3ν mixing, namely, for nonzero values of the mixing angle θ_{13}. We also present updated bounds (as of June 2003) in the 3ν parameter space $(\delta m^2, \theta_{12}, \theta_{13})$.

In our KamLAND data analysis [35], we use the absolute spectrum of events reported in [23], taken above a background-safe analysis threshold of 2.6 MeV in visible energy E. The events below such threshold might contain a significant component of geological $\overline{\nu}_e$'s [36], whose large normalization uncertainties are poorly constrained at present by the KamLAND data themselves [23]. Above 2.6 MeV, a total of 54 events is found, against 86.8 events expected from reactors [23]. Finally, the observed energy spectrum of events is analyzed as in [24], with the improvements

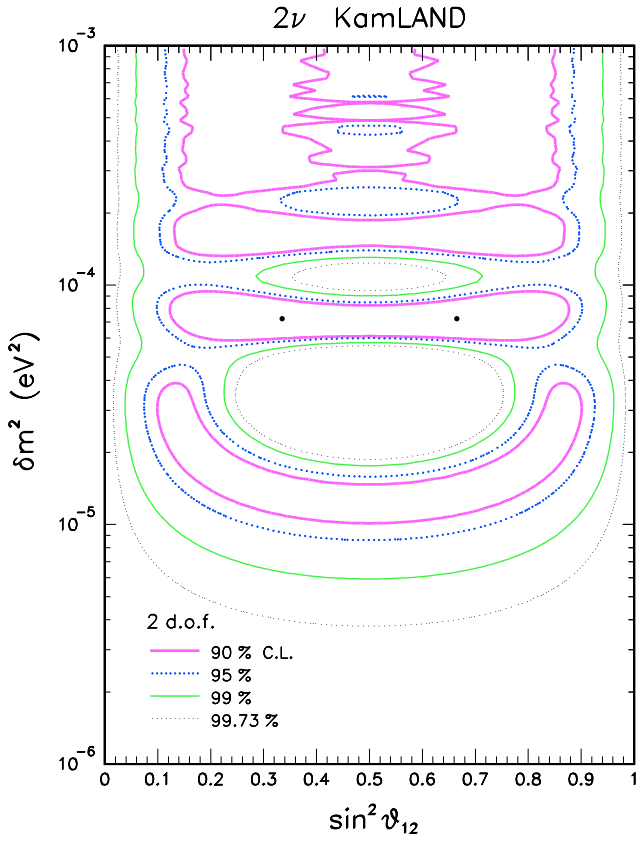

Figure 5: *Two-flavor active neutrino oscillations: Analysis of the KamLAND energy spectrum data above 2.6 MeV in the* $(\delta m^2, \sin^2\theta_{12})$ *parameter space. A "tower" of octant-symmetric regions is allowed at different values of* δm^2*. The symmetric best fits are indicated by black dots. The left dot is remarkably close to the solar best fit in Fig. 4.*

reported in [35].

An updated 2ν analysis of current solar+CHOOZ neutrino data, [24], is presented here. The fit includes 81 solar neutrino observables [30, 24] and 14 CHOOZ spectrum bins [21, 24], for a total of 95 data points. The $\Delta\chi^2$ expansion around the minimum, relevant for the estimation of the oscillation parameters $(\delta m^2, \sin^2\theta_{12})$, is shown in Fig. 4, where we have restricted the δm^2 range to the only three decades relevant for the LMA solution and for the following KamLAND analysis.

In Fig. 5 we report the 2ν analysis of KamLAND [35]: there appears to be a "tower" of solutions which tend to merge and become indistinguishable for increasing δm^2; the lower three ones are, however, rather well separated at 90% C.L. Notice that our allowed regions are slightly larger (i.e., less constraining) than those in the rate+shape analysis of [23]. One of the two octant-symmetric

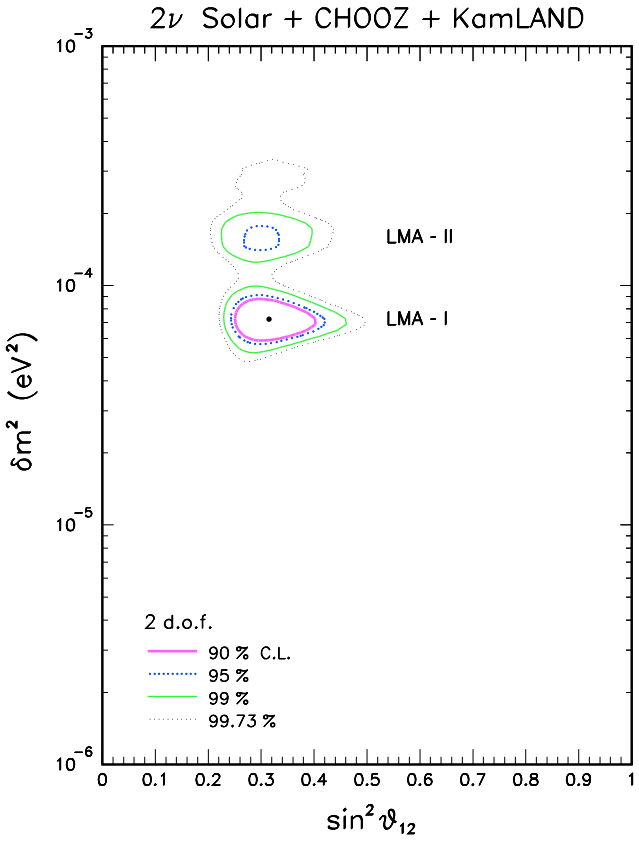

Figure 6: *Two-flavor active neutrino oscillations: Global analysis of solar, CHOOZ, and KamLAND neutrino data in the* $(\delta m^2, \sin^2\theta_{12})$ *parameter space. With respect to Fig. 4, the LMA region is significantly restricted, and appears to be split into two sub-regions (LMA-I and LMA-II), well-separated at 99% C.L.*

best fits points in Fig. 5 (black dots) is remarkably close to the best fit in Fig. 4. The difference in location with respect to the KamLAND official best-fit point at $(\delta m^2/\mathrm{eV}^2, \sin^2\theta_{12}) = (6.9 \times 10^{-5},\, 0.5)$ [23] is not statistically significant, amounting to a variation $\Delta\chi^2 \ll 1$.

The combination of the solar+CHOOZ results in Fig. 4 with the KamLAND results in Fig. 5 gives the global 2ν results shown in Fig. 6. Two rather distinct solutions, that we label LMA-I and LMA-II, are seen to emerge. The LMA-I solution is clearly preferred by the data, being close to the best fit points of both solar+CHOOZ and KamLAND data. The LMA-II solution is located at a δm^2 value about twice as large as for the LMA-I, but is separated from the latter by a modest $\Delta\chi^2 = 5.4$ difference (dominated by solar neutrino data). Indeed, if we conservatively demand a 99.73% C.L. for the allowed regions, the LMA-I and LMA-II solutions appear to merge (and extend towards $\delta m^2 \sim 3 \times 10^{-4}$ eV^2) in a single broad solution. In any case, at any chosen C.L., the allowed regions of Fig. 6 are

significantly smaller than those in Fig. 4. Therefore, with just 54 initial events, the KamLAND experiment is not only able to select the LMA region as *the* solution to the solar neutrino problem, but can also significantly restrict the corresponding oscillation parameter space. With several hundred events expected in the forthcoming years, there are thus very good prospects to refine the parameter estimate [24].

4 Indications of matter effects in the Sun

Within the LMA region, solar neutrino oscillations are governed not only by the kinematical mass-mixing parameters $(\delta m^2, \theta_{12})$, but should also be significantly affected by the interaction energy difference $(V = V_e - V_a)$ between ν_e's and ν_a's propagating in the solar (and possibly Earth) background matter [31, 32], through the so-called Mikheev-Smirnov-Wolfenstein (MSW) mechanism [31] in adiabatic regime [33]. Although Earth matter effects (i.e., day-night variations of solar event rates) remain elusive, solar matter effects seem to emerge, at least indirectly, from the combination of the available data (and especially from SNO), through a preference for an average oscillation probability smaller than 1/2 at energies of a few MeV. A phenomenological approach to the problem has been recently presented in [34], where a free parameter $a_{\rm MSW}$ is introduced, called to modulate the overall amplitude of the interaction energy difference V in the dynamical term $\mathcal{H}_{\rm dyn}$ of the Hamiltonian,

$$V \to a_{\rm MSW} \cdot V \ . \tag{3}$$

By treating $a_{\rm MSW}$ as a continuous parameter, one can try to constrain its allowed range through global data analyses: A preference for $a_{\rm MSW} \sim O(1)$ would then provide an indirect indication for the occurrence of matter effects with standard size, as opposed to the case of pure "vacuum" oscillations ($\mathcal{H}_{\rm dyn} \simeq 0$).

We have verified that the current solar neutrino data, by themselves, place only very loose and uninteresting limits on $a_{\rm MSW}$, as far as the mass-mixing oscillation parameters are left unconstrained. In fact, since the oscillation physics depends mostly on the ratio V/k, where $k = \delta m^2/2E$ is the neutrino oscillation wavenumber, a variation of the kind $V \to a_{\rm MSW} V$ is largely absorbed by a similar rescaling of k (i.e., of δm^2). In order to break this degeneracy, we need to include explicitly an experiment which is highly sensitive to δm^2 and basically insensitive to matter effects, such as KamLAND.

A SSM-independent preference for $P_{ee} < 1/2$ has been provided first by the combination of SNO CC and SK data [14] and then by SNO data alone through the CC/NC double ratio [15], but not yet with a significance high enough to rule out

$P_{ee} = 1/2$ [30]. Let us consider, in particular, the latest SNO constraints in the plane $(\Phi_e, \Phi_{\mu\tau})$ charted by the solar ν_e and $\nu_{\mu,\tau}$ fluxes, as shown in Fig. 3 of the original SNO paper [15]. In such a figure, although the SNO best-fit point clearly prefers $P_{ee} \sim 1/3$ (corresponding to $\Phi_{\mu\tau} \simeq 2\Phi_e$), the 95% C.L. ellipse is still compatible with $P_{ee} \sim 1/2$ (namely, $\Phi_{\mu\tau} \simeq \Phi_e$). However, future SNO NC and CC data can considerably improve the constraints on P_{ee}, by reducing both the statistical and the systematic error on the CC/NC ratio [37].

In conclusion, although the combination of all current solar neutrino data suggests a pattern of P_{ee} compatible with the LMA energy profile and indicates an overall preference for the first octant of θ_{12} [16], the emerging indications in favor of solar matter effects from this data set are not strongly compelling yet.

Until now we have illustrated how a single datum (the SNO CC/NC double ratio) can discriminate the case of standard matter effects ($a_{\rm MSW} = 1$) from the case of zeroed matter effects ($a_{\rm MSW} = 0$) in the LMA parameter region. By using further experimental information from KamLAND, one could try to test [34] whether the "solar + KamLAND" combination of data can constrain matter effects in the Sun to have the right size [$a_{\rm MSW} \sim O(1)$]. In this kind of analyses, KamLAND basically fixes the oscillation parameters $(\delta m^2, \sin^2\theta_{12})$, and thus the kinetic part of the Hamiltonian, $\mathcal{H}_{\rm kin}$. The role of solar neutrino data is then to check that the overall amplitude $a_{\rm MSW}$ of the interaction energy difference V in the dynamical term $\mathcal{H}_{\rm dyn}$ is consistent with the standard electroweak model ($a_{\rm MSW} = 1$).

We have thus performed global analyses including both current solar neutrino data and current (or prospective) KamLAND data, with $(\delta m^2, \sin^2\theta_{12}, a_{\rm MSW})$ unconstrained. In particular, the analysis of current KamLAND data is based on the binned energy spectrum of reactor neutrino events observed above 2.6 MeV (54 events) [23]. Prospective KamLAND spectral data have instead been generated, with the same energy threshold and binning, by assuming either the LMA-I best-fit point ($\delta m^2 = 7.3 \times 10^{-5}$ eV^2 and $\sin^2\theta_{12} = 0.315$) or the LMA-II best-fit point ($\delta m^2 = 15.4 \times 10^{-5}$ eV^2 and $\sin^2\theta_{12} = 0.300$) [25], and increased statistics (5×54 and 10×54 events). The CHOOZ reactor data [21] are also included.

Figure 7 shows the results of such global fits, in terms of the function $\Delta\chi^2 = \chi^2 - \chi^2_{\rm min}$ for variable $a_{\rm MSW}$ and unconstrained (i.e., minimized away) mass-mixing parameters. The $n\sigma$ bounds on $a_{\rm MSW}$ are then given by $\Delta\chi^2 = n^2$. Let us focus first on the solid curve, which refers to the fit with *current* KamLAND data. It appears that such curve can already place $> 3\sigma$ upper and lower bounds on $a_{\rm MSW}$. In particular, the hypothetical case of zeroed matter effects is already disfavored at $\sim 3.5\sigma$, thus providing an indirect indication in favor of matter effects in the Sun.

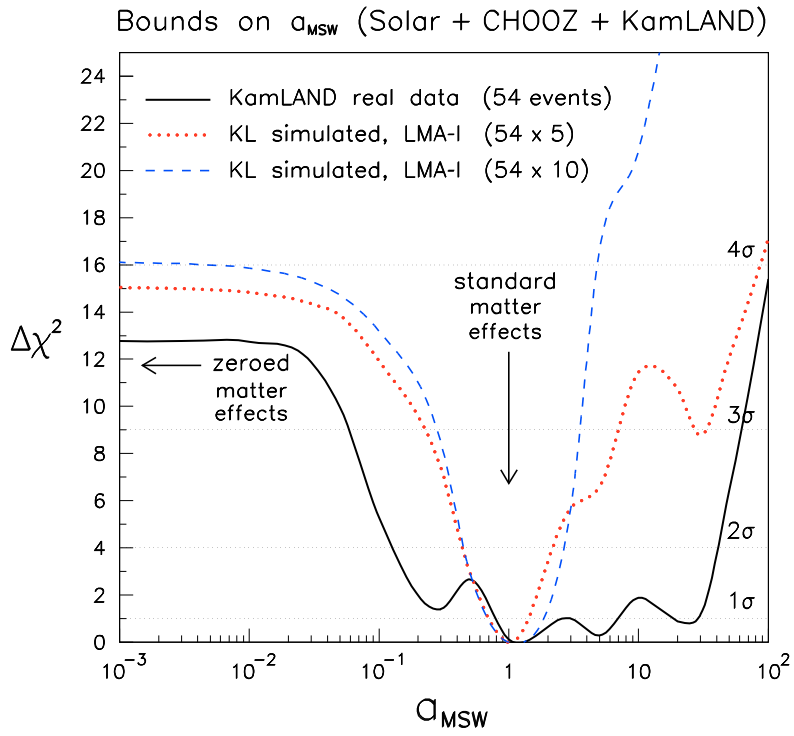

Figure 7: *Bounds on* $a_{\rm MSW}$ *for unconstrained* $(\delta m^2, \sin^2\theta_{12})$*, including current solar and CHOOZ neutrino data, as well as current or prospective KamLAND data. The solid curve refers to the fit including current KamLAND spectrum data above 2.6 MeV threshold (54 events), and shows that the hypothetical case of zeroed matter effects is already disfavored. The other curves refer to simulated KamLAND data, generated by assuming the LMA-I solution, and statistics increased by a factor of five (dotted curve) and of ten (dashed curve).*

The best-fit value of $a_{\rm MSW}$ is close to the standard prediction ($a_{\rm MSW} = 1$). However, the overall $\pm 3\sigma$ range for $a_{\rm MSW}$, spanning about three orders of magnitude, is rather large. The width of this range can be understood by recalling the following facts: (1) the LMA range of δm^2 constrained by solar neutrino data, which covers about one decade [30, 24], can be shifted up or down by shifting $a_{\rm MSW}$ with respect to 1, since the LMA oscillation physics depends on $V/k \propto a_{\rm MSW}/\delta m^2$; (2) the range of δm^2 constrained by current terrestrial data (including KamLAND+CHOOZ), which covers about two decades [25], is much less affected by $a_{\rm MSW}$ variations. As a consequence, by appropriately shifting $a_{\rm MSW}$, it is possible to overlap the reconstructed ranges of δm^2 from solar and from reactor data over about $1 + 2$ decades. When the overlap sweeps through the degenerate δm^2 intervals allowed by KamLAND alone [25], the fit is locally improved, leading to a "wavy" structure in the $\Delta\chi^2$. In conclusion, although current solar+reactor data strongly disfavor

$a_{\rm MSW} = 0$ (zeroed matter effects) and provide a best fit close to $a_{\rm MSW} = 1$ (standard matter effects), the presence of other local minima in the $\Delta\chi^2$ function, as well as the broad 3σ allowed range for $a_{\rm MSW}$, do not allow to claim a clear evidence of standard matter effects from current data.

The broken curves in Fig. 7 refer to prospective KamLAND data, generated by assuming as true solution the LMA-I best-fit point. The energy threshold, the binning, and the systematic uncertainties are assumed to be the same as for the current KamLAND data. The dotted (dashed) curve refers to a number of reactor neutrino events five (ten) times larger than the current statistics. It can be seen that the global fit will progressively constrain $a_{\rm MSW}$ within one decade at $\pm 3\sigma$ and, most importantly, will lead to a marked preference for $a_{\rm MSW} \simeq 1$, which is not yet evident in the present data. In conclusion, if the LMA-I solution is the true one, there are good prospect to test unambiguously the occurrence and size of standard matter effects in the Sun.

5 Conclusions

We have analyzed in detail the current SK atmospheric neutrino data and and the first K2K spectral data, in order to review the status of standard $\nu_\mu \to \nu_\tau$ oscillations. We have then provided updated bounds for the standard oscillation parameters. In particular, the statistical analysis of the uncertainties reveals that K2K will lead further progress in this field, especially through higher-statistics tests of the low-energy spectrum bins.

Going to solar neutrinos, the KamLAND experiment has clearly selected the LMA region as the solution to the solar neutrino problem, and has further reduced the $(\delta m^2, \sin^2\theta_{12})$ parameter space for active neutrino oscillations. In the 2ν case, we find that the post-KamLAND LMA solution appears to be basically split into two sub-regions, LMA-I and LMA-II. The LMA-I solution, characterized by $\delta m^2 \sim 7 \times 10^{-5}$ eV^2 and $\sin^2\theta_{12} \sim 0.3$, is preferred by the global fit. The LMA-II solution represents the second best fit, at about twice the value of δm^2.

In the simplest picture, solar neutrino oscillations depend on the kinematical parameters $(\delta m^2, \sin^2\theta_{12})$ and on standard dynamical MSW effects in matter. These effects in current solar neutrino data are starting to emerge through an increasingly marked preference for $P_{ee} < 1/2$, but still remain not clearly identified. In order to quantify statistically the occurrence of MSW effects, we have introduced a free parameter $a_{\rm MSW}$ modulating the amplitude of the ν interaction energy difference in the neutrino evolution equation. By treating $a_{\rm MSW}$ as a continuous parameter, we

have then performed a global analysis including current solar, CHOOZ, and KamLAND data. The results are encouraging, since upper and lower bounds on $a_{\rm MSW}$ appear to emerge at the $> 3\sigma$ level. In particular, the case of "zeroed" matter effects is significantly disfavored. Moreover, the best-fit is tantalizingly close to the standard expectations for matter effects ($a_{\rm MSW} = 1$).

The situation will improve through higher KamLAND statistics. In both the LMA-I and LMA-II cases, it appears possible to reduce the current uncertainty on $a_{\rm MSW}$ by about two orders of magnitude. In conclusion, the selection of a single solution in the LMA oscillation parameter space appears to be crucial, before any definite conclusion can be made on the emerging indications of standard matter effects in the Sun.

6 Acknowledgments

G.L.F. thanks the organizers of the Conference for the kind ospitality. This work is co-financed by the Italian Ministero dell'Università e della Ricerca Scientifica e Tecnologica (MURST) within the "Astroparticle Physics" project.

References

1. SK Collaboration, Y. Fukuda *et al.*, Phys. Rev. Lett. **81**, 1562 (1998) [hep-ex/9807003].

2. T. Kajita and Y. Totsuka, Rev. Mod. Phys. **73**, 85 (2001).

3. SK Collaboration, M. Shiozawa *et al.*,, in *Neutrino 2002,* Proceedings of the 20th International Conference on Neutrino Physics and Astrophysics (Munich, Germany, 2002), to appear.

4. MACRO Collaboration, M. Ambrosio *et al.*, Phys. Lett. B **517**, 59 (2001).

5. Soudan 2 Collaboration, W.W. Allison *et al.*, Phys. Lett. B **449**, 137 (1999).

6. K2K Collaboration, S.H. Ahn *et al.*, Phys. Lett. B **511**, 178 (2001).

7. K2K Collaboration, M.H. Ahn *et al.*, Phys. Rev. Lett. **90**, 041801 (2003).

8. Homestake Collaboration, B.T. Cleveland, T. Daily, R. Davis Jr., J.R. Distel, K. Lande, C.K. Lee, P.S. Wildenhain, and J. Ullman, Astrophys. J. **496**, 505 (1998).

9. SAGE Collaboration, J.N. Abdurashitov *et al.*, J. Exp. Theor. Phys. **95**, 181 (2002) [Zh. Eksp. Teor. Fiz. **95**, 211 (2002)].

10. GALLEX Collaboration, W. Hampel *et al.*, Phys. Lett. B **447**, 127 (1999).

11. T. Kirsten for the GNO Collaboration, in *Neutrino 2002*, 20th International Conference on Neutrino Physics and Astrophysics (Munich, Germany, 2002).

12. SK Collaboration, S. Fukuda *et al.*, Phys. Rev. Lett. **86**, 5651 (2001); *ibidem*, 5656 (2001).

13. SK Collaboration, S. Fukuda *et al.*, Phys. Lett. B **539**, 179 (2002).

14. SNO Collaboration, Q.R. Ahmad *et al.*, Phys. Rev. Lett. **87**, 071301 (2001).

15. SNO Collaboration, Q.R. Ahmad *et al.*, Phys. Rev. Lett. **89**, 011301 (2002).

16. SNO Collaboration, Q.R. Ahmad *et al.*, Phys. Rev. Lett. **89**, 011302 (2002).

17. J.N. Bahcall, M.H. Pinsonneault, and S. Basu, Astrophys. J. **555**, 990 (2001).

18. B. Pontecorvo, Zh. Eksp. Teor. Fiz. **53**, 1717 (1968) [Sov. Phys. JETP **26**, 984 (1968)].

19. Z. Maki, M. Nakagawa, and S. Sakata, Prog. Theor. Phys. **28**, 870 (1962).

20. See, e.g., the reviews: S.M. Bilenky, C. Giunti, and W. Grimus, Prog. Part. Nucl. Phys. **43**, 1 (1999); P. Langacker, in *NOW 2000*, Proceedings of the Neutrino Oscillation Workshop 2000 (Conca Specchiulla, Italy, 2000), ed. by G.L. Fogli, Nucl. Phys. Proc. Suppl. **100**, 383 (2001); M. C. Gonzalez-Garcia and Y. Nir, Rev. Mod. Phys. 75, 345 (2003).

21. CHOOZ Collaboration, M. Apollonio *et al.*, Phys. Lett. B **466**, 415 (1999); M. Apollonio *et al.*, hep-ex/0301017, to appear in Eur. Phys. J. C.

22. Palo Verde Collaboration, F. Boehm *et al.*, Phys. Rev. D **64**, 112001 (2001).

23. KamLAND Collaboration, K. Eguchi *et al.*, Phys. Rev. Lett. **90**, 021802 (2003).

24. G.L. Fogli, G. Lettera, E. Lisi, A. Marrone, A. Palazzo, and A. Rotunno, Phys. Rev. D **66**, 093008 (2002).

25. G.L. Fogli, E. Lisi, A. Marrone, D. Montanino, A. Palazzo, and A. Rotunno, hep-ph/0212127, submitted to Phys. Rev. D.

26. G.L. Fogli, E. Lisi, A. Marrone and D. Montanino, Phys. Rev. D **67**, 093006 (2003)

27. G.L. Fogli, E. Lisi, A. Marrone, and G. Scioscia, Phys. Rev. D **59**, 033001 (1999).

28. G.L. Fogli, E. Lisi, and A. Marrone, Phys. Rev. D **64**, 093005 (2001).

29. G.L. Fogli, E. Lisi, and A. Marrone, Phys. Rev. D **65**, 073028 (2002).

30. G.L. Fogli, E. Lisi, A. Marrone, D. Montanino and A. Palazzo, Phys. Rev. D **66**, 053010 (2002).

31. L. Wolfenstein, Phys. Rev. D **17**, 2369 (1978); S.P. Mikheev and A.Yu. Smirnov, Yad. Fiz. **42**, 1441 (1985) [Sov. J. Nucl. Phys. **42**, 913 (1985)].

32. V.D. Barger, K. Whisnant, S. Pakvasa, and R.J.N. Phillips, Phys. Rev. D **22**, 2718 (1980).

33. L. Wolfenstein, in *Neutrino '78*, 8th International Conference on Neutrino Physics and Astrophysics (Purdue U., West Lafayette, Indiana, 1978), ed. by E.C. Fowler (Purdue U. Press, 1978), p. C3.

34. G.L. Fogli, E. Lisi, A. Palazzo, and A.M. Rotunno, Phys. Rev. D **67**, 073001 (2003) [hep-ph/0211414].

35. G.L. Fogli, E. Lisi, A. Marrone, D. Montanino, A. Palazzo, and A.M. Rotunno Phys. Rev. D **67**, 073002 (2003).

36. L.M. Krauss, S.L. Glashow, and D.N. Schramm, Nature **310**, 191 (1984).

37. A. Hallin for the SNO Collaboration, in *Neutrino 2002* [11].